ORIGINAL PAPER

Ni-in-garnet geothermometry in mantle rocks: a high pressure experimental recalibration between 1100 and 1325 °C

Z. J. Sudholz[1] · G. M. Yaxley[1] · A. L. Jaques[1] · J. Chen[2]

Abstract

The temperature-dependent exchange of Ni and Mg between garnet and olivine in mantle peridotite is an important geothermometer for determining temperature variations in the upper mantle and the diamond potential of kimberlites. Existing calibrations of the Ni-in-garnet geothermometer show considerable differences in estimated temperature above and below 1100 °C hindering its confident application. In this study, we present the results from new synthesis experiments conducted on a piston cylinder apparatus at 2.25–4.5 GPa and 1100–1325 °C. Our experimental approach was to equilibrate a Ni-free Cr-pyrope-rich garnet starting mixture made from sintered oxides with natural olivine capsules ($Ni_{olv} \cong 3000$ ppm) to produce an experimental charge comprised entirely of peridotitic pyrope garnet with trace abundances of Ni (10–100 s of ppm). Experimental runs products were analysed by wave-length dispersive electron probe microanalysis (EPMA) and laser ablation inductively coupled plasma mass spectrometry (LA-ICP-MS). We use the partition coefficient for the distribution of Ni between our garnet experimental charge and the olivine capsule $\left(lnD^{Ni}_{grt/olv}; \frac{Ni_{grt}}{Ni_{olv}} \right)$, the Ca mole fraction in garnet (X^{Ca}_{grt}; Ca/ (Ca + Fe + Mg)), and the Cr mole fraction in garnet (X^{Cr}_{grt}; Cr/(Cr + Al)) to develop a new formulation of the Ni-in-garnet geothermometer that performs more reliably on experimental and natural datasets than existing calibrations. Our updated Ni-in-garnet geothermometer is defined here as:

$$T(°C) = \frac{-8254.568}{\left(\left(X^{Ca}_{grt} \times 3.023 \right) + \left(X^{Cr}_{grt} \times 2.307 \right) + \left(lnD^{Ni}_{\frac{grt}{olv}} - 2.639 \right) \right)} - 273 \pm 55$$

where $D^{Ni}_{grt/olv} = \frac{Ni_{grt}}{Ni_{olv}}$, Ni is in ppm, $X^{Ca}_{grt} = Ca/(Ca + Fe + Mg)$ in garnet, and $X^{Cr}_{grt} = Cr/(Cr + Al)$ in garnet. Our updated Ni-in-garnet geothermometer can be applied to garnet peridotite xenoliths or monomineralic garnet xenocrysts derived from disaggregation of a peridotite source. Our calibration can be used as a single grain geothermometer by assuming an average mantle olivine Ni concentration of 3000 ppm. To maximise the reliability of temperature estimates made from our Ni-in-garnet geothermometer, we provide users with a data quality protocol method which can be applied to all garnet EPMA and LA-ICP-MS analyses prior to Ni-in-garnet geothermometry. The temperature uncertainty of our updated calibration has been rigorously propagated by incorporating all analytical and experimental uncertainties. We have found that our Ni-in-garnet temperature estimates have a maximum associated uncertainty of ± 55 °C. The improved performance of our updated calibration is demonstrated through its application to previously published experimental datasets and on natural, well-characterised garnet peridotite xenoliths from a variety of published datasets, including the diamondiferous Diavik and Ekati kimberlite pipes from the Lac de Gras kimberlite field, Canada. Our new calibration better aligns temperature estimates using the Ni-in-garnet geothermometer with those estimated by the widely used (Nimis and Taylor, Contrib Mineral Petrol 139:541–554, 2000) enstatite-in-clinopyroxene geothermometer, and confirms an improvement in performance of the new calibration relative to existing versions of the Ni-in-garnet geothermometer.

Communicated by Othmar Müntener.

Extended author information available on the last page of the article

Introduction

The partitioning of Ni between garnet and olivine in peridotite is strongly dependent on temperature and has been used to formulate several empirical (Griffin et al. 1989; Ryan et al. 1996) and experimental (Canil 1994, 1999) geothermometers. Since its first formulation, the Ni-in-garnet geothermometer has been an important tool for studying the nature of the upper mantle (e.g. Griffin et al. 1999, 2004) and for determining the diamond potential of kimberlites (Griffin and Ryan 1995). The different calibrations of the Ni-in-garnet geothermometer provide similar temperature estimates between 1050 and 1150 °C but differ considerably outside of this range (Fig. 1). The empirical Ni-in-garnet geothermometer of Ryan et al. (1996) was calibrated using the O'Neill and Wood (1979) olivine-garnet Fe–Mg exchange geothermometer applied to natural peridotite xenoliths; whereas, the Canil (1999) Ni-in-garnet geothermometer was experimentally calibrated using natural and Ni-doped starting materials at near solidus and sub-solidus temperatures, typically at high pressure (> 4 GPa). Above 1200 °C the Ryan et al. (1996) empirical calibration provides a higher estimated temperature than the Canil (1999) experimental calibration; whereas, below 900 °C the Ryan et al. (1996) calibration provides a lower equilibration temperature than the experimental calibration. The Ryan et al. (1996) calibration likely incorporates many of the well-known problems associated with the O'Neill and Wood (1979) geothermometer (see below for "Discussion"). Despite this both calibrations of the Ni-in-garnet geothermometer continue to be used in studies of garnet xenocrysts to estimate mantle temperatures, with the Ryan et al. (1996) calibration commonly preferred in studies assessing the diamond potential of kimberlites.

In the following study we revisit the Ni-in-garnet geothermometer using a novel experimental and analytical approach. We present the results for nine new Ni partitioning experiments conducted between a Ni-free Cr-pyrope-rich garnet sintered oxide starting mixture and a natural Ni-bearing olivine capsule. Our experiments were conducted at pressures (P) and temperatures (T) from 2.25 to 4.5 GPa and 1100 to 1325 °C. The experimental run products were analysed by EPMA and high precision LA-ICP-MS. The results have been used to formulate an updated Ni-in-garnet geothermometer with improved reliability relative to the existing calibrations and better alignment with temperature estimates from pyroxene geothermometry.

Methods

Experimental methods

A Ni-free Cr-pyrope-rich garnet composition was used as the starting material for all experiments (Table 1). This starting material is based on the composition of a model mantle peridotite (MORB-Pyrolite) garnet, but recalculated to contain no Ni (Green 2015; Sudholz et al. 2021). Because our garnet starting composition did not contain Ni, it was anticipated that the Ni-free garnet starting mixture and the olivine capsule would equilibrate to produce an experimental charge comprised entirely of monomineralic garnet with trace levels of Ni. Our 'synthesis' approach based on diffusion to calibrating the Ni-in-garnet thermometer differs from the original experimental method presented in Canil (1994, 1999) in that we do not use equilibrium brackets as experimental reversals using our technique poses additional experimental difficulties. The Ni-free garnet starting

Fig. 1 Comparison between the Canil (1999) and Ryan et al. (1996) Ni-in-garnet geothermometer calibrations. Temperature for Canil (1999) geothermometer was calculated using a Ni olivine concentration of 3250 ppm, 3000 ppm, and 2750 ppm
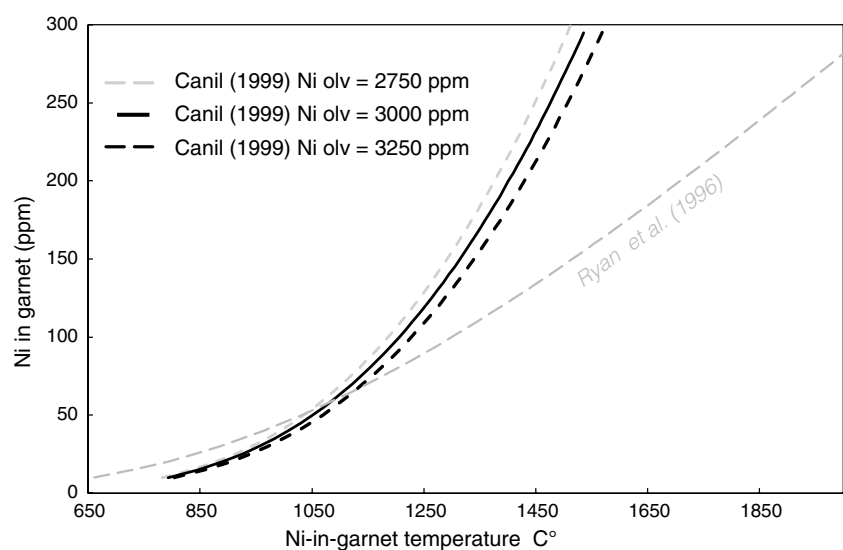
Table 1 Composition of the Ni-free pyrolite garnet starting mixture used in all experiments reported in this study, and a representative analysis of the San Carlos olivine used as capsule in this study

Oxide (wt%)	Ni-free Cr-pyrope-rich garnet starting composition	San Carlos olivine capsule
SiO_2	42.2	39.66
TiO_2	0.28	< 0.01
Al_2O_3	22.84	< 0.01
FeO	6.88	10.04
MnO	0.19	0.13
MgO	20.51	49.90
CaO	5.36	0.07
Na_2O	0.04	< 0.01
Cr_2O_3	1.70	0.02
NiO	0.00	0.38
Total	100.00	100.23
Mg#	84	89

$Mg\# = Mg/(Mg+Fe) \times 100$

composition was prepared by grinding sintered oxide (FeO, SiO_2, Al_2O_3, TiO_2, MgO, MnO, Cr_2O_3) and carbonate (Na_2CO_3, $CaCO_3$) powders under acetone and then firing at 1000 °C to decarbonate the mix (Yaxley and Green 1998). Only the oxide components listed in Table 1 were included in our Ni-free garnet starting composition. The Ni-free garnet starting composition was loaded into a capsule fabricated from gem-quality commercial San Carlos olivine which naturally contained approximately 2800–3200 ppm Ni. A typical major element composition of the San Carlos olivine used for our capsules is listed in Table 1. The outside diameter (OD) of the olivine capsule was 2.3 mm and the inside diameter of the bore containing the garnet starting material was 1 mm. The height of the olivine capsule was typically 2.5 mm. The bore within the olivine capsule that contained the garnet starting composition was typically 0.5–1 mm deep. An olivine disk was used as a lid with a typical thickness of 0.5 mm. The olivine capsule assembly was placed within a 3.5 mm OD $Ag_{0.5}Pd_{0.5}$ or Pt capsule, which was arc-welded shut on both ends. The length of the metal capsule was typically < 4 mm. A half-inch NaCl ± Pyrex assembly with a graphite furnace was used for all experiments. Further details of this assembly are given in Sudholz et al. (2021). An illustration of the experimental assembly used in this study is shown in Fig. 2. A 200-tonne end-loaded piston cylinder apparatus was used for all experiments. The experimental pressure and temperature of this apparatus has been calibrated by the quartz–coesite transition (Bose and Ganguly 1995). Experimental temperature was measured using a type-B Pt–Rh thermocouple. The temperature and pressure of experiments ranged between 1100–1325 °C and 2.25–4.5 GPa. The run duration of all experiments was
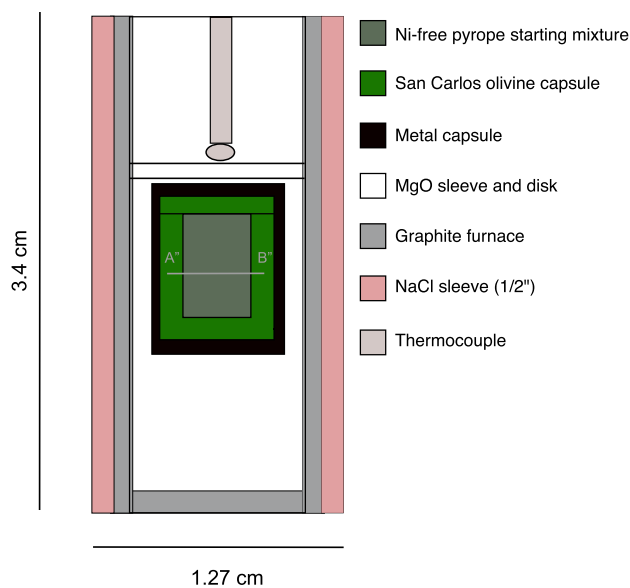
Fig. 2 Simplified illustration of the experimental assembly used in this study. The exact dimensions of assembly interior are not to scale. The typical length and orientation of a LA-ICP-MS traverse for each experiment is label as A"–B" (see text for discussion)

120 h. The oxygen fugacity of all experiments was buffered to the graphite furnace and is thus approximately equivalent to the graphite–oxygen (CCO) buffer reaction. Under these conditions the oxygen fugacity of our experiments was too low for appreciable oxidation of Fe^{2+} in the Ni-free garnet starting composition (Holloway et al. 1992). The run conditions and assemblages for each experiment are listed in Table 2. In preparation for imaging and quantitative analysis, the metal capsules were removed from their assemblies, mounted in epoxy resin and polished down to expose the garnet experimental charge and the olivine capsule. They were re-impregnated with epoxy under vacuum to seal any cracks. Capsules were polished down to a ¼ µm grit using a diamond lap and coated with a thin film of carbon for EPMA. This film was removed for analysis by LA-ICP-MS.

Table 2 Summary of experimental run conditions

Experiment	T °C	P GPa	Duration (hours)	Metal capsule
NIMPY5	1100	3	120	$Ag_{0.5}Pd_{0.5}$
NIMPY4	1150	3.5	120	$Ag_{0.5}Pd_{0.5}$
NIMPY9	1175	4	120	$Ag_{0.5}Pd_{0.5}$
NIMPY27	1175	2.5	120	Pt
NIMPY10	1200	3	120	$Ag_{0.5}Pd_{0.5}$
NIMPY7	1225	4	120	$Ag_{0.5}Pd_{0.5}$
NIMPY28	1275	4.5	120	Pt
NIMPY12	1300	4	120	Pt
NIMPY13	1325	4	120	Pt

Analytical methods

The concentration of major elements in the olivine capsule and garnet experimental charge were measured on a JEOL JXA-8530F+EPMA at the Centre for Advanced Microscopy, The Australian National University. An accelerating voltage of 10 or 15 kV, a beam current of 20 nA, and a beam diameter less than 1 µm were used routinely for most analyses. Analytical standards were a mix of synthetic and natural *ASTIMEX Mineralogy* standards as follows: Na (albite), Mg (periclase and olivine), Al (sanidine and pyrope), Si (sanidine and diopside), Ca (diopside), Ti (rutile), Cr (chromite), Mn (rhodonite), Fe (hematite and magnetite), and Ni (pentlandite). Counting times were typically 20 s (peak and background) for major elements and 30–40 s for minor elements with a total analytical time of approximately 2–3 min. The data correction was done using the 'PAP model' (Pouchou and Pichoir 1991). Approximately 15–25 analyses were performed on garnet grains within the experimental charge of each sample. Similarly, 5–30 analyses were typically performed on the olivine capsule within each sample. Olivine analyses were performed across the entire capsule, and garnet analyses were performed across the entire experimental charge. Most garnet grains synthesised from our Ni-free garnet starting mixture were well-equilibrated based on stoichiometry. However, to ensure only homogenous garnet compositions were included in our experimental dataset, garnet analyses with totals < 98 wt% and > 101 wt %, and cation totals < 7.96 and > 8.04 (calculated on the basis of twelve oxygens in garnet) were rejected. This filtering resulted in the removal of less than two or three garnet analyses in each experiment.

The concentrations of trace elements in the garnet experimental charge were measured by LA-ICP-MS on an Agilent Technologies 7700 quadrupole mass spectrometer coupled to a Lambda Physik (λ = 193 nm) laser ablation system at the Research School of Earth Sciences, The Australian National University. All samples were ablated in a Helix sample cell with the laser operating at a 5 Hz pulse rate, 80 mJ output energy, and 22 µm diameter spot. Data acquisition involved a background (Ar-gas blank) pre- and post- ablation for 25 s. A traverse across the entire garnet experimental charge was used to maximise the total ablation time. The ablation profile typically commenced within the olivine capsule, passing through the entire garnet experimental charge and back out into the olivine capsule at the opposite end of the assembly (see Fig. 2). The length of each LA-ICP-MS traverse was typically between 500 and 1500 µm. The garnet experimental charge was comprised of numerous individual garnet grains of varying size. A typical LA-ICP-MS traverse through our experiments is labelled on Fig. 2 by the A"–B" notation. The isotopes measured within the garnet experimental change were: ^{23}Na, ^{27}Al, ^{55}Mn, ^{45}Sc, ^{49}Ti, ^{51}V,

^{53}Cr, ^{55}Mn, ^{59}Co, ^{60}Ni and ^{71}Ga. Garnet Al concentrations determined by EPMA were used as the internal standard and the NIST reference glass SRM 612 (NIST 612) (Jochum et al. 2011) was used as the primary standard. Reference glasses BCR-2G and NIST 610 were monitored as secondary standards. Standard measurements bracketed each traverse across the garnet experimental charge. Several traverses were completed across each sample, typically in varying directions. Each traverse contained between 50 and 400 individual ablations points across the garnet experimental charge. The data obtained were reduced using the Iolite v2.3 software package (Paton et al. 2011). The Ni concentrations in garnet used in our calibration were taken from the averages of representative sections of the LA-ICP-MS traverse across the garnet experimental charge. These representative sections did not include analyses on the olivine capsule, nor any garnet analyses that were in close proximity to the boundary with the olivine capsule, or regions of the traverse that intersected epoxy-filled cracks within the charge. The representative sections of each traverse were assessed based on homogenous Al and Ni concentrations in garnet. A typical LA-ICP-MS traverse across the experimental charge for sample NIMPY10 is shown in Fig. 3. The slope between the garnet experimental charge and olivine capsule observed on Fig. 3 were a result of minor laser overlap and were observed within all experiments: these portions of each LA-ICP-MS traverse (and the olivine capsule analyses to the far right and left) were not used as part of our calibration.

Results

Our experiments were successful at synthesising an experimental charge comprised entirely of monomineralic Cr-pyrope garnet with trace levels (10–100 s of ppm) of Ni. The experimental charge was positioned within the olivine capsule (Fig. 4) and was made up of numerous garnet grains that ranged in size from 10 to > 35 um. Garnet grains presented well-formed crystal faces that were typically free of zoning. Some garnets in a few runs showed minor core to rim chemical zonation (Fig. 5). Analyses showed that the zonation was predominantly caused by minor variation in the concentration of Cr and Ti, which approached equilibrium at a slower rate due to the slower diffusion rates of these elements with respect to the divalent cations (e.g. Carlson 2012). A representative analysis on the core and rim of a zoned garnet from experiment NIMPY9 is highlighted in Table 3. The olivine capsule retained its original shape and did not display evidence of compositional variation in backscattered electron images. The high-temperature experiments at 4 GPa contained a very minor amount of an additional phase, found along the grain boundaries of olivine and occasionally alongside garnet at the interface with the olivine

Fig. 3 Representative LA-ICP-MS traverse showing the change in Al and Ni concentration between the garnet experimental charge and the olivine capsule (labelled). LA-ICP-MS traverse is for experiment NIMPY10. Individual points represent a single LA-ICP-MS ablation measurement
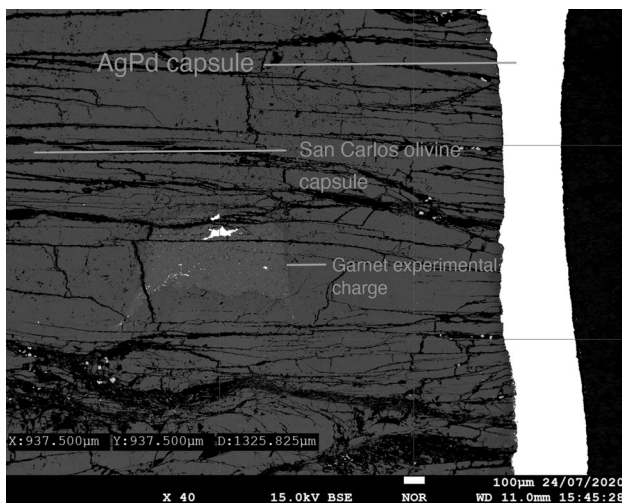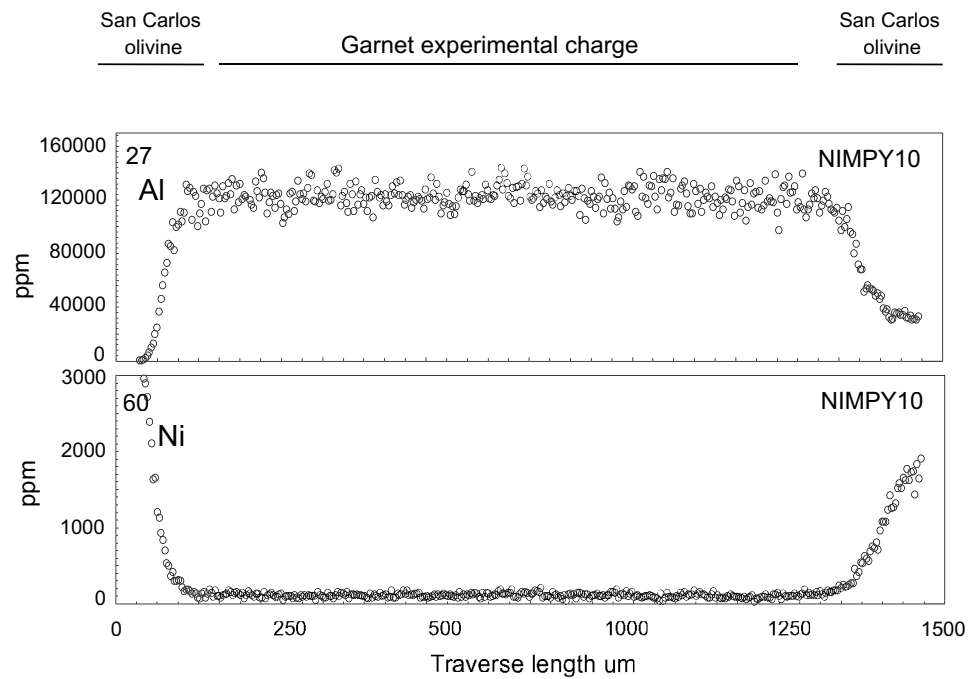

Fig. 4 Back-scattered electron image of the monomineralic garnet experimental charge, olivine capsule, and metal ($Ag_{0.5}Pd_{0.5}$) capsule for sample NIMPY4. Note scale of 100 μm. Bright inclusions across the interior of Fig. 4 are pieces of the metal ($Ag_{0.5}Pd_{0.5}$) capsule that were etched into the sample during polishing. These metal pieces were avoided and did not affect the quality of EPMA and/or LA-ICP-MS analyses

Fig. 5 Back-scattered electron image of the interface between the garnet experimental charge and the olivine capsule. Note scale of 10 μm

capsule. The grains were typically too small (<3 μm) for precise WDS analyses; however, energy-dispersive spectra confirmed that it contained Mg, Fe and Ca. We interpret this material as Fe-bearing dolomite, indicative of the presence of minor carbon in our experiments. The source of carbon is unknown but may relate to traces of residual organic volatiles associated with the preparation of the sintered oxide
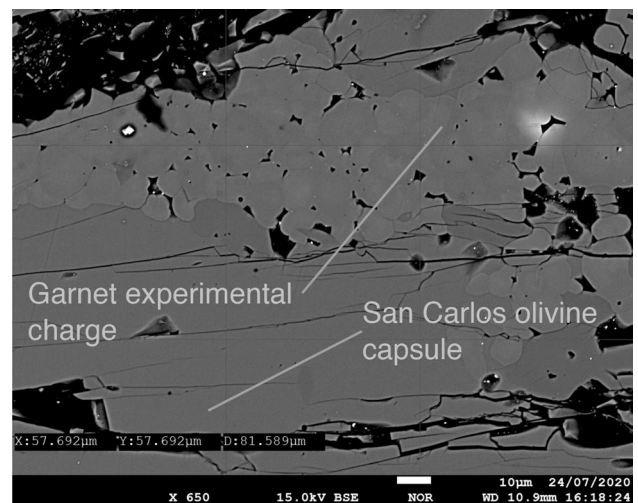
garnet mix. The averages of the major oxide concentrations measured by EPMA in garnet for each experiment are listed in Table 3. The concentration of MgO and NiO in garnet measured by EPMA increased with increasing temperature; whereas, CaO, TiO_2 and FeO decreased with increasing temperature. The concentration of FeO and MgO in garnet ranged between 5.9–7.5 wt% and 20.7–23.6 wt% respectively. The concentration of Cr_2O_3 typically ranged between 1.50 and 1.85 wt% and decreased marginally from the starting composition (<0.30 wt%). The concentration of CaO in garnet typically ranged between 4.0 and 5.0 wt% in the

Table 3 Average concentration of major and minor oxides in garnet (wt%)

Experiment	n	SiO$_2$	SD	TiO$_2$	SD	Al$_2$O$_3$	SD	FeO	SD	MnO	SD	MgO	SD	CaO	SD	Na$_2$O	SD	Cr$_2$O$_3$	SD	NiO	SD	Total	X$_{grt}^{Mg}$
NIMPY5	23	42.06	0.45	0.22	0.06	22.86	0.06	7.16	0.53	0.22	0.01	21.02	0.75	4.88	0.49	0.03	0.01	1.63	0.17	0.02	0.01	100.09	83.9
NIMPY4	19	42.30	0.35	0.18	0.06	23.14	0.06	7.49	0.16	0.24	0.01	21.44	0.46	4.50	0.58	0.03	0.01	1.62	0.19	0.01	0.01	100.97	83.6
NIMPY9	15	41.42	0.24	0.27	0.05	22.72	0.05	7.46	0.22	0.24	0.03	20.69	0.33	5.14	0.37	0.08	0.01	1.79	0.66	0.01	0.01	99.81	83.1
NIMPY27	17	41.81	0.58	0.16	0.02	23.03	0.02	6.53	0.30	0.24	0.02	21.85	0.37	4.06	0.30	0.01	0.01	1.67	0.14	0.02	0.01	99.40	85.6
NIMPY10	22	42.20	0.32	0.21	0.05	22.96	0.05	6.61	0.25	0.23	0.02	21.25	0.58	4.79	0.66	0.02	0.01	1.54	0.20	0.02	0.01	99.84	85.1
NIMPY7	21	42.16	0.51	0.18	0.06	22.95	0.06	6.50	0.46	0.25	0.01	22.01	0.61	4.07	0.71	0.07	0.02	1.63	0.22	0.02	0.01	99.84	85.7
NIMPY28	23	42.38	0.29	0.19	0.02	22.59	0.02	5.93	0.48	0.24	0.01	23.56	0.66	2.73	0.57	0.02	0.01	1.80	0.16	0.02	0.01	99.48	87.6
NIMPY12	18	42.59	0.47	0.15	0.01	22.88	0.01	6.29	0.27	0.24	0.01	23.38	0.59	2.56	0.94	0.16	0.14	1.62	0.10	0.01	0.03	99.87	86.8
NIMPY13	13	42.40	0.26	0.13	0.02	22.90	0.02	7.06	0.20	0.27	0.01	23.46	0.48	2.36	0.74	0.01	0.01	1.85	0.10	0.03	0.01	100.48	85.5
Core—NIMPY9	2	41.92	0.24	0.34	0.02	21.28	0.02	9.60	1.11	0.26	0.01	18.45	0.87	5.66	0.06	0.04	<0.01	2.52	0.04	0.01	<0.01	100.10	77.3
Rim—NIMPY9	2	42.75	0.36	0.23	0.02	22.65	0.02	7.64	0.02	0.23	0.02	20.14	0.17	4.84	0.28	0.07	0.01	1.62	0.09	<0.01	<0.01	100.49	82.6

Standard deviations are reported to 1σ. Representative analyses of a rim and core on a zoned garnet grain are presented for experiment NIMPY9

n number of EPMA analyses, *SD* standard deviation

experiments at ~ 3 GPa and the lower temperature (1175 °C) experiment at 4 GPa. The CaO concentration in garnet in the 4 GPa experiments showed a marked decrease to < 3 wt% CaO in the high-temperature experiments (NIMPY28, NIMPY12, NIMPY13). Garnet from these experiments also exhibited slightly lower TiO$_2$, FeO, as well as higher concentrations of MgO, and Cr$_2$O$_3$. The small changes in CaO abundance in garnet with increasing temperature were presumably accommodated by undetectable (using EPMA) changes in CaO abundance in the much more voluminous olivine capsule for the ~ 3 GPa experiments. LA-ICP-MS was used to measure the trace concentration of eleven elements in the garnet experimental charge (see "Analytical methods"). The majority of the trace elements were not included in the starting oxide composition and have been incorporated into the garnet experimental charge through a series of exchange reactions with the olivine capsule during the experimental runs. The concentration of Ni in garnet ranged from 67 to 180 ppm and increased linearly with increasing temperature. The concentration of Ni within most samples varied by ± 25 ppm. The concentration of Ga ranged from < 5 to > 15 ppm and decreased with increasing temperature. The concentration of Co and Sc varied from 24 to 100 ppm and 4 to 70 ppm respectively. The concentration of Ti varied from 300 to 1200 ppm and decreased strongly with increasing temperature. The average concentration of trace elements in garnet for each representative section of the LA-ICP-MS traverse for each experiment, along with their standard deviations are shown in Table 4.

The concentrations of major and minor oxides in the olivine capsule were measured by EPMA only. The concentration of MgO and FeO in olivine ranged from 49 to 51 wt% and 8 to 10 wt%, respectively. The concentration of FeO decreased marginally with increasing experimental temperature. The variation in the concentration of MgO in the olivine capsules did not deviate with temperature. The X$_{olv}^{Mg}$ varied between approximately 0.89 and 0.92. The olivine adjacent to the metal capsule did not show any major variations in the concentration of FeO which suggest that our experiments were not affected by zoning within the olivine. The concentration of Al$_2$O$_3$ and Cr$_2$O$_3$ in the olivine both increased with increasing temperature. The concentration of NiO typically ranged between 0.37 and 0.42 wt%, equivalent to 2800 and 3200 ppm, and did not show any systematic variation with changing experimental temperature, nor with position across the capsule. The averages of the major oxide concentrations measured by EPMA of the olivine used for the capsule assemblage and the capsule for each experiment are listed in Table 5.

A close approach to chemical equilibrium between the garnet experimental charge and olivine capsule in terms of Ni partitioning is indicated in our experiments by the uniform Ni concentrations in the olivine and garnets in each

Table 4 Average concentration of trace elements in garnet for the representative portions of the LA-ICPMS traverses for each experiment used in our updated calibration of the Ni-in-garnet geothermometer

Experiment	P GPa		n	Ni	SD	Ti	SD	Mn	SD	Na	SD	Co	SD
NIMPY5	3	1100	34	67.31	18	1363	157	1631	111	542	142	23.86	4.62
NIMPY4	3.5	1150	40	89.55	19	950	113	1789	93	317	86	32.70	4.74
NIMPY4	3.5	1150	18	94.53	21	1019	115	1765	106	506	155	31.81	5.69
NIMPY9	4	1175	30	92.58	23	1374	195	1672	94	1296	847	28.18	4.36
NIMPY9	4	1175	24	97.80	24	1412	204	1742	158	1437	342	28.44	5.82
NIMPY27	2.5	1175	33	95.02	22	732	136	1658	107	112	86	26.66	4.64
NIMPY27	2.5	1175	33	89.04	22	732	147	1674	131	174	96	28.32	5.00
NIMPY27	2.5	1175	31	84.46	21	722	125	1704	108	95	61	28.01	5.10
NIMPY10	3	1200	62	99.31	26	1206	159	1665	90	370	104	31.23	4.09
NIMPY10	3	1200	252	104.9	29	1238	204	1648	122	468	179	30.42	5.74
NIMPY10	3	1200	22	102.6	27	1222	183	1704	106	562	139	30.37	6.79
NIMPY7	4	1225	291	124.2	26	1094	155	1753	111	2771	965	36.64	5.96
NIMPY7	4	1225	73	128.0	22	1077	141	1745	89	2756	699	36.42	5.41
NIMPY7	4	1225	57	126.7	23	1080	151	1737	100	2098	515	36.56	6.49
NIMPY28	4.5	1275	66	132.5	26	1015	176	1785	93	442	510	31.74	5.68
NIMPY28	4.5	1275	37	125.6	25	913	140	1857	209	124	71	35.99	5.43
NIMPY28	4.5	1275	50	116.8	29	1016	147	1788	190	330	337	34.06	6.54
NIMPY12	4	1300	19	175.9	28	1151	199	1954	242	1596	277	47.37	5.55
NIMPY12	4	1300	27	170.2	32	1104	208	1979	176	1143	496	50.99	8.61
NIMPY12	4	1300	47	173.6	32	1045	206	1862	154	4552	721	48.07	7.69
NIMPY13	4	1325	44	172.0	40	367	74	374	24	878	428	101.67	9.75
NIMPY13	4	1325	39	181.9	35	335	61	367	39	550	291	108.91	18.71
NIMPY13	4	1325	42	179.8	41	304	52	341	25	1553	693	130.09	23.13

Experiment	Sc	SD	V	SD	Cr	SD	Ga	SD
NIMPY5	7.70	4.00	33.60	7.43	11,089	762	11.10	5.25
NIMPY4	11.95	3.75	27.51	4.61	10,305	487	13.40	4.53
NIMPY4	9.56	3.31	27.39	3.55	10,377	365	13.95	6.63
NIMPY9	4.15	4.38	29.45	6.07	10,752	732	13.53	5.15
NIMPY9	7.50	4.57	30.51	6.12	10,884	878	14.70	6.26
NIMPY27	13.08	5.88	34.25	5.78	10,697	690	6.57	6.20
NIMPY27	8.61	4.26	28.08	6.80	10,166	688	8.20	3.62
NIMPY27	12.13	4.40	29.53	7.24	9755	628	6.97	4.10
NIMPY10	11.53	5.25	36.29	5.59	11,101	820	11.66	5.28
NIMPY10	10.37	4.89	38.87	9.35	10,900	952	11.61	5.42
NIMPY10	9.56	4.66	33.00	5.18	10,945	749	12.58	5.38
NIMPY7	16.96	6.18	32.37	6.65	10,149	798	12.42	5.47
NIMPY7	16.76	5.83	32.08	5.74	9934	732	12.76	4.81
NIMPY7	14.34	5.87	38.15	17.88	10,275	731	14.13	5.83
NIMPY28	6.95	3.09	31.26	6.54	11,128	3106	15.08	5.91
NIMPY28	20.53	6.18	38.76	5.96	10,429	787	9.93	4.12
NIMPY28	8.79	4.03	34.79	8.34	11,399	1183	11.43	5.60
NIMPY12	36.79	7.32	43.01	8.93	10,020	538	8.28	3.45
NIMPY12	31.56	8.90	49.76	9.09	10,334	717	9.29	5.44
NIMPY12	31.72	7.14	41.57	9.02	10,271	706	8.72	4.15
NIMPY13	42.86	12.73	86.45	18.88	370.37	29.68	30.70	11.29
NIMPY13	48.99	16.34	86.77	39.27	355.80	42.14	31.25	14.73
NIMPY13	69.41	20.26	100.15	20.41	331.50	29.45	37.52	20.74

Table 4 (continued)

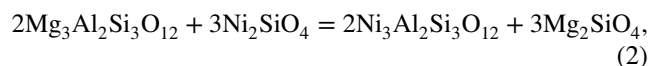Note several traverses were performed across each sample

SD standard deviation at a 1σ level, *n* number of individual ablation analyses along a LA-ICP-MS traverse

charge, revealed by the LA-ICPMS traverses across the samples (Fig. 3). Our results are in excellent agreement with the previous experimental Ni-partitioning results of Canil (1994, 1999) (see below), which used a different experimental technique. The Canil (1999) Ni-in-garnet geothermometer applied to our experimental run products gave temperature estimates typically within ± 25 °C of the experimental temperature (Table 6). The largest discrepancies (ca. ± 50 °C) between the calculated and experimental temperatures were typically observed in our high-temperature (> 1300 °C) experiments (Table 6). An additional indicator of equilibrium in our experiments is the concentration of Al_2O_3 in the olivine capsules. Equilibration temperatures calculated using the experimentally calibrated Al-in-olivine geothermometer of Bussweiler et al. (2017) typically reproduced our experimental temperatures to better than 50 °C for the runs at temperatures ≥ 1200 °C and better than 100 °C for the lower temperature runs (where the EPMA analyses of Al_2O_3 in olivine were subject to larger errors). This indicates equilibrium was also achieved in terms of partitioning of Al from the garnet in the charge into the enclosing olivine capsule. In addition, equilibrium in terms of Fe–Mg partitioning between olivine and garnet is indicated for our lower temperature experiments using the O'Neill and Wood (1979) garnet–olivine Fe–Mg geothermometer. Larger differences (≥ 200 °C) between the estimated and our experimental temperature were observed in our highest temperature experiments. The reason for this is not clear but could reflect a small amount of Fe-loss or the presence of minor Fe^{3+}. Previous studies have shown that the Fe–Mg olivine–garnet geothermometer reproduces experimental temperatures (e.g. Brey and Köhler 1990) to $\pm \sim 110$ °C (Canil and O'Neill 1996) but larger differences (~ 200 °C) can occur, especially in natural peridotites when compared with other (pyroxene) geothermometers due to the presence of Fe^{3+} in garnet (Canil and O'Neill 1996; Nimis and Grütter, 2010; Matjuschkin et al. 2014). The presence of significant Fe^{3+} in our experimental garnets is unlikely as they do not show any major cation deficits or excesses on the X^{2+} or X^{3+} crystallographic sites, and our experiments equilibrated under oxygen fugacity conditions (buffered by the graphite furnace to $\approx$CCO) not conducive to appreciable Fe^{2+} oxidation. However, we cannot rule out the presence of trace or minor amounts of Fe^{3+} in the garnets. Another possible reason for the apparent departures from olivine–garnet Fe–Mg equilibrium in some of our higher temperature experiments might be a small amount of Fe loss to the Pt capsule. This is suggested in several of our higher temperature runs where both
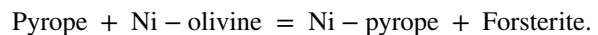
the garnet and olivine have lower FeO (higher Mg-value) than their starting compositions (notably NIMPY28). However, the good agreement between our experimental results and those of Canil (1999) using different experimental techniques, coupled with the partitioning of Al between garnet and the olivine capsule, even for the samples suspected of minor Fe loss, indicates that equilibrium was maintained with respect to Ni (and Al) partitioning regardless.

Discussion

The temperature-dependent exchange of Ni and Mg between garnet and olivine in peridotite is defined by Eq. (2), whereby pyrope reacts with Ni–olivine to produce Ni–pyrope and forsterite:

$$2Mg_3Al_2Si_3O_{12} + 3Ni_2SiO_4 = 2Ni_3Al_2Si_3O_{12} + 3Mg_2SiO_4, \tag{2}$$

Or

$$Pyrope + Ni - olivine = Ni - pyrope + Forsterite.$$

Assuming ideal mixing, the partitioning of Ni and Mg between garnet and olivine can be expressed as $D_{grt/olv}^{Ni/Mg}$ (Eq. 3):

$$D_{grt/olv}^{Ni/Mg} = \frac{(Ni/Mg)_{grt}}{(Ni/Mg)_{olv}}, \tag{3}$$

where Ni and Mg are in ppm.

As expected the $D_{grt/olv}^{Ni/Mg}$ for our experiments contains a strong temperature dependence with no resolvable pressure dependence. The latter observation for our experiments is consistent with the small volume change for the exchange reaction defining the geothermometer of ~ 0.13 J/bar (Canil 1994). The small variation in the concentration of MgO in garnet and olivine for our experiments allow $D_{grt/olv}^{Ni/Mg}$ to be simplified to of $D_{grt/olv}^{Ni}$. The concentrations of CaO and Cr_2O_3 in garnet are expected to have some minor influence on Ni partitioning between garnet and olivine in peridotite. We have accounted for the effects of CaO and Cr_2O_3 in garnet for the following reasons. Calcium has a significant impact on the Fe–Mg partitioning between olivine and garnet (O'Neill and Wood 1979). CaO solubility in olivine in garnet peridotites is temperature- (and pressure) dependent (Köhler and Brey 1990; De Hoog et al. 2010) and, most importantly, our experiments and those of Canil (1999) show a linear dependence of $D_{grt/olv}^{Ni}$ with

Table 5 Average concentration of major and minor oxides in olivine capsules (wt%)

Experiment	n	SiO$_2$	SD	TiO$_2$	SD	Al$_2$O$_3$	SD	FeO	SD	MnO	SD	MgO	SD	CaO	SD	Na$_2$O	SD	Cr$_2$O$_3$	SD	NiO	SD	Total	X$^{Mg}_{olv}$
San Carlos	15	39.66	0.64	0.01	<0.01	0.01	<0.01	10.04	0.20	0.13	0.01	49.90	0.15	0.07	<0.01	0.01	0.01	0.02	<0.01	0.38	0.02	100.23	89.8
NIMPY5	30	40.49	0.20	0.01	<0.01	0.02	<0.01	9.21	0.14	0.10	0.01	49.52	0.34	0.07	0.01	0.02	0.01	0.04	0.02	0.41	0.01	99.88	90.5
NIMPY4	58	40.77	0.33	0.01	0.01	0.04	0.03	9.46	0.47	0.13	0.02	49.27	0.63	0.06	0.01	0.04	0.08	0.04	0.03	0.40	0.03	100.21	90.2
NIMPY9	33	41.04	0.86	0.01	<0.01	0.05	0.01	9.14	0.29	0.10	0.01	49.25	0.76	0.06	0.01	0.03	0.02	0.05	0.01	0.42	0.02	100.15	90.5
NIMPY27	14	41.03	0.26	0.01	<0.01	0.05	<0.01	9.20	0.54	0.12	0.02	49.64	0.48	0.09	0.01	0.01	0.01	0.04	0.02	0.38	0.02	100.56	90.5
NIMPY10	5	40.48	0.54	0.01	0.01	0.02	0.01	9.68	0.23	0.14	0.01	49.03	0.36	0.09	0.02	0.01	0.01	0.06	0.01	0.41	0.01	99.92	90
NIMPY7	6	37.52	1.33	0.01	<0.01	0.05	0.01	9.87	0.33	0.13	0.01	51.44	0.36	0.09	0.01	0.03	0.02	0.05	0.02	0.45	0.02	99.63	90.2
NIMPY28	10	40.30	0.47	0.01	<0.01	0.02	0.01	8.09	0.26	0.13	0.02	50.28	0.53	0.08	0.03	0.04	0.01	0.03	0.01	0.37	0.02	99.34	91.7
NIMPY12	18	41.01	0.31	0.01	0.01	0.04	0.01	9.20	0.42	0.12	0.01	49.50	0.28	0.08	0.01	0.03	0.02	0.02	0.02	0.40	0.02	100.41	90.5
NIMPY13	11	40.43	0.44	0.01	<0.01	0.04	0.01	10.64	0.15	0.15	0.01	48.21	0.45	0.06	0.01	0.02	0.01	0.03	0.01	0.37	0.01	99.95	88.9

Standard deviations are reported to 1σ

n number of EPMA analyses, *SD* standard deviation

X^{Ca}_{grt}. This strong linear association between $D^{Ni}_{grt/olv}$ and X^{Ca}_{grt} is likely a result of interactions of Ca on Ni–Mg partitioning between garnet and olivine. Similarly, our experimental data also show a correlation between X^{Cr}_{grt} and $\ln D^{Ni}_{grt/olv}$. This correlation is due to the close association between X^{Ca}_{grt} and X^{Cr}_{grt} in garnet-bearing peridotites (Grütter et al. 2004) and reflects additional mixing interactions taking place within garnet. Cr_2O_3 substitution in olivine has been shown to be inversely correlated with temperature in both natural peridotites (De Hoog et al. 2010) and in high-pressure experimental studies of fertile peridotite composition (Bussweiler et al. 2017). The pressure dependence of Cr_2O_3 and CaO in peridotitic garnet has previously been discussed by Grütter et al. (2004 and refs therein) and, thus, including X^{Ca}_{grt} and X^{Cr}_{grt} in the Ni-in-garnet geothermometer formulation should help account for any minor unresolved pressure dependence on $\ln D^{Ni}_{grt/olv}$ and result in an improved calibration of the Ni-in-garnet geothermometer.

The temperature dependence of $\ln D^{Ni}_{grt/olv}$ for our experiments can be rearranged into an expression for temperature through multiple linear regression of X^{Ca}_{grt} and X^{Cr}_{grt} and $1/T$ (K). We found the following expression for T (°C) best reproduced the temperature of our experimental dataset:

$$T(°C) = \frac{-8254.568}{\left(\left(X^{Ca}_{grt} \times 3.023 \right) + \left(X^{Cr}_{grt} \times 2.307 \right) + \left(\ln D^{Ni}_{\frac{grt}{olv}} - 2.639 \right) \right)} - 273 \pm 55,$$

(4)

where $D^{Ni}_{grt/olv} = \frac{Ni_{grt}}{Ni_{olv}}$, Ni is in ppm, $X^{Ca}_{grt} = Ca/(Ca + Fe + Mg)$ in garnet, and $X^{Cr}_{grt} = Cr/(Cr + Al)$ in garnet.

Our geothermometer equation (Eq. 4) was fit to our experimental data with an R^2 of 0.97 which, on average, reproduced the experimental temperature of our dataset within 12 °C at a 1σ standard deviation of 10 °C. Our updated calibration (Eq. 4) performed well when applied to the Canil (1994, 1999) experimental datasets, reproducing the experimental temperature of these experiments within 75 °C (Fig. 6), in some cases better than the Canil (1999) calibration. Large differences (± 100 °C) between our Ni-in-garnet estimated temperature and the Canil (1994, 1999) experimental temperature were most commonly observed at high temperature (> 1300 °C). These experiments were also poorly reproduced by the Canil (1999) Ni-in-garnet geothermometer. Incorporation of the Canil (1994 and 1999) experimental datasets into our calibration model did not improve the overall fit of our regression equation and these were therefore not included in the final regression equation.

Table 6 Comparison of calculated temperature of equilibration for our experimental run products using various single grain and two-phase geothermometers

Experiment	Experimental T °C	Experimental P GPa	T Buss	T Canil	T Ryan	T OW
NIMPY5	1100	3	1148	1101	1134	1191
NIMPY4	1150	3.5	1283	1177	1262	1207
NIMPY9	1175	4	1326	1172	1277	1166
NIMPY27	1175	2.5	1248	1178	1249	1354
NIMPY10	1200	3	1155	1195	1311	1452
NIMPY7	1225	4	1339	1225	1417	1510
NIMPY28	1275	4.5	1235	1286	1411	1455
NIMPY12	1300	4	1298	1347	1607	1582
NIMPY13	1325	4	1276	1384	1625	1705

All geothermometer temperature estimates are reported in T °C

Geothermometers. OW = O'Neill and Wood (1979) garnet–olivine Fe–Mg geothermometer; Canil = Ni-in-garnet geothermometer (Canil 1999); Buss = Bussweiler et al. (2017); Ryan = Ryan et al. (1996) Ni-in-garnet geothermometer. Temperature estimates for OW, and Buss geothermometers were determined using garnet and olivine EPMA data reported in Tables 3 and 5. Temperature estimates for the Canil (1999) Ni-in-garnet geothermometer used Ni garnet data reported in Table 4, using a Ni olivine concentration 3000 ppm. The Ni-in-garnet temperature estimate for each sample are presented as averages from estimates made using Table 5 data

Fig. 6 Application of our updated Ni-in-garnet geothermometer to the experimental datasets of Canil (1994) and Canil (1999). Our Ni-in-garnet geothermometer has been applied to all Canil (1994, 1999) experiments that have a reported value for $\ln D^{Ni}_{grt/olv}$, regardless of the Ni concentration in garnet. Dashed line is ± 100 °C of the experimental temperature. Error on Ni-in-garnet temperature estimates are ± 55 °C
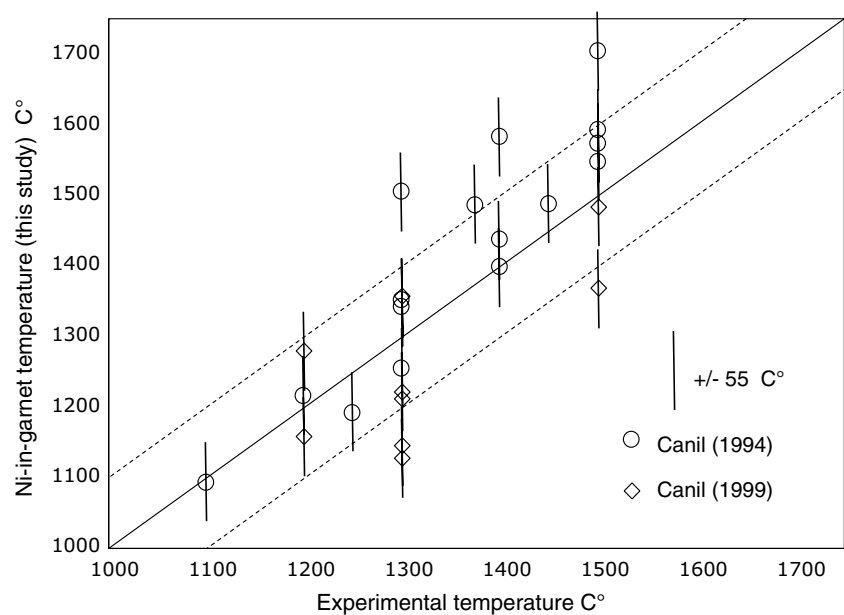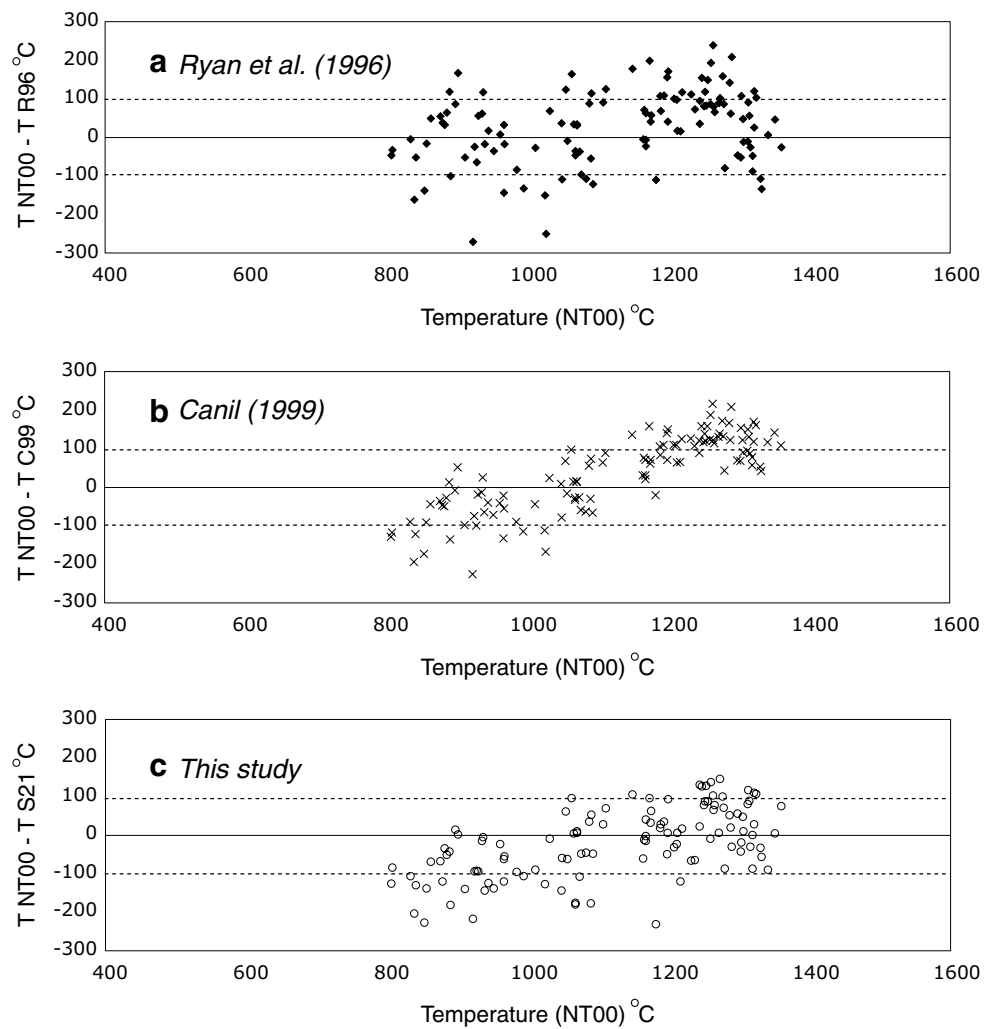
Propagation of uncertainties

The experimental temperature, EPMA and LA-ICP-MS analyses used to calibrate our updated Ni-in-garnet geothermometer are all subject to small but cumulative uncertainties. To accurately assess the true uncertainty on temperature estimates made by our Ni-in-garnet geothermometer we have propagated all experimental and analytical uncertainties. This approach provides a more robust and realistic uncertainty value compared to the common practise of compounding EPMA standard deviation values

(see Sudholz et al. 2021). In Eq. (4) uncertainties exist in the experimental temperature measured by the Pt–Rh thermocouple, the analysis of CaO, FeO, MgO, Cr$_2$O$_3$, and Al$_2$O$_3$ in garnet by WDS on EPMA, and the analysis of Ni by LA-ICP-MS. The Pt–Rh thermocouple used to measure the temperature of our experiments has an uncertainty of ~ 1%. Using the conventional WDS EPMA analytical procedure described above, the maximum uncertainty in the measured major oxide concentrations of CaO, FeO, MgO, Cr$_2$O$_3$, and Al$_2$O$_3$ in garnet were 0.58%, 0.63%, 0.37%, 3.62%, and 0.44%, respectively. These uncertainty values were obtained by performing ten repeated

measurements on an *ASTIMEX Mineralogy* pyrope standard. The uncertainty for each major oxide was determined by dividing the standard deviation by the average concentration (σ1 level). The measurement of trace levels (10–100 s of ppm) of Ni in garnet using LA-ICP-MS is subject to an extremely low degree of uncertainty (< 1%). The uncertainty (in percentage) in estimated temperature for our updated Ni-in-garnet geothermometer calibration was determined by taking the square root of the sum of the squares of these errors (in percentage), which is defined by the following equation:

$$\delta T = \sqrt{(\delta Texp)^2 + (\delta CaO)^2 + (\delta FeO)^2 + (\delta MgO)^2 + (\delta Cr_2O_3)^2 + (\delta Al_2O_3)^2 + (\delta Ni)^2},$$

where Texp = experimental temperature, and δ = uncertainty in percentage.

This approach results in a temperature estimate uncertainty of 4.02%, which is equivalent to a maximum temperature uncertainty of ± 55 °C.

Data quality protocols

To maximise the reliability of our updated Ni-in-garnet geothermometer we recommend applying the following data quality protocols to garnet analyses prior to performing Ni-in-garnet geothermometry:

1) *Quality of EPMA data*

Garnet analyses with oxide totals below 98 wt% or above 102 wt%, or with cation totals less than 7.97 or greater than 8.03 cpfu (per 12 oxygen atoms) should be excluded from Ni-in-garnet temperature calculations. As well as avoiding inferior analyses a limit of 8.03 cations should exclude garnets with high Fe^{3+} which may be metasomatised as most mantle garnets have Fe^{3+}/total Fe of 0.02–0.15 (e.g. Luth et al. 1990).

2) *Equilibration with olivine*

Our updated Ni-in-garnet geothermometer should only be applied to garnet grains which equilibrated in the presence of olivine. For garnet xenocrysts, we recommend applying the Grütter et al. (2004) 'G-number classification' to ensure that eclogitic and pyroxenitic garnet analyses are omitted from any Ni-in-garnet temperature calculations. Ni-in-garnet temperature estimates on single-grain garnet xenocryst that contain less than 1 wt% Cr_2O_3 and/or fall within fields G0, G4, and G3 of Fig. 7 of Grütter et al. (2004) should be interpreted with caution.

3) *Temperature range*

Ni-in-garnet temperature estimates that are extensively outside of the range of the original calibration should be interpreted with caution. In particular, Ni-in-garnet temperature estimates below 700 °C and above 1400 °C should be carefully assessed.

4) *Ni garnet concentration range*

Garnet Ni concentrations below 10 ppm and above 200 ppm should be excluded from Ni-in-garnet temperature calculations. In addition, we recommend that the concentration of Ni in garnet should preferentially be measured by LA-ICP-MS, particularly for xenolith samples which may be affected by secondary fluorescence from Ni in adjacent olivine grains. An EPMA may be used to measure the concentration of Ni in single-grain garnet xenocrysts, however a prolonged counting time and higher beam current is recommended.

Application to mantle peridotite xenolith suites

To evaluate the performance of our updated calibration of the Ni-in-garnet geothermometer against the Ryan et al. (1996) and Canil (1999) calibrations, we have compiled a large dataset of LA-ICP-MS and EPMA analyses for garnet and clinopyroxene derived from peridotite xenoliths. Our dataset includes 117 xenoliths, which includes samples from Udachnaya (Ionov et al. 2010; Yaxley et al. 2012; Agashev et al. 2013; Doucet et al. 2015), Diavik, (Creighton et al. 2010), Letlhakane (Van Achterbergh et al. 2001) Wesselton (Hanger et al. 2015), Finsch (Gibson et al. 2008), Dalnyaya (Ashchepkov et al. 2017), Vitim (Ionov 2004), Zagadonchnaya (Ziberna et al. 2013), Premier (Viljoen et al. 2009) and several pipes throughout eastern China (Zheng et al. 2006) and the Kaapvaal Craton (Grégoire et al. 2003; Viljoen et al. 2005; Le Roex and Class 2016). The garnet in our dataset were typically lherzolitic in origin (G9 of Grütter et al. 2004). For each sample, we have calculated the equilibration temperature for garnet using the Ryan et al. (1996), Canil (1999), and our updated calibration (Eq. 4). All Ni-in-garnet

temperature estimates for the Canil (1999) calibration and our updated calibration (Eq. 4) were made assuming a fixed olivine concentration of 3000 ppm, which is similar to the value proposed by Ryan et al. (1996) of 2900 ± 360 ppm as representative of the Ni concentration in olivine from typical cratonic mantle peridotite. We have also calculated the equilibration pressure and temperature for clinopyroxene in each xenolith using the widely used Nimis and Taylor (2000) enstatite-in-clinopyroxene geothermometer and the recently experimentally recalibrated chromium-in-clinopyroxene geobarometer (Sudholz et al. 2021) which improves the performance of the geobarometer at pressures above 4.5 GPa. The Nimis and Taylor (2000) enstatite-in-clinopyroxene geothermometer is regarded as one of the most reliable geothermometers for garnet peridotite xenoliths (Nimis and Grütter 2010) and has an estimated uncertainty of ± 30°C. All clinopyroxene analyses and pressure–temperature estimates used in our dataset were filtered according to protocols recommended by Sudholz et al. (2021). The clinopyroxene and garnet analyses for the xenoliths in our dataset, as well as the pressure and temperature estimates using the geothermobarometers are provided in Supplementary File 1.

The Nimis and Taylor (2000) and Sudholz et al. (2021) pressure and temperature estimates for our dataset ranged from 1.75 GPa to above 8 GPa, and 800 to 1360 °C. The majority of pressure and temperature estimates were between 4–6 GPa and 1000–1200 °C. The temperature difference between the Ryan et al. (1996) calibration of the Ni-in-garnet geothermometer and the Nimis and Taylor (2000) enstatite-in-clinopyroxene geothermometer (NT00-R96) varied from < 10 °C to > 250 °C (Fig. 7a). No systematic variation is evident with the Ryan et al (1996) temperatures. The variation in NT00-R96 did not show any resolvable correlation with pressure. The temperature difference between the Canil (1999) calibration and the Nimis and Taylor (2000) enstatite-in-clinopyroxene geothermometer (NT00-C99) was typically ± 150 °C (Fig. 7b). Between 850–1350 °C the NT00-C99 exhibited a distinct positive slope. At face value this slope suggests that the Canil (1999) geothermometer calibration potentially slightly overestimates temperature below 850 °C and underestimates temperature above 1150 °C relative to NT00. Differences at low temperatures between the temperatures derived from the Ni-in-garnet geothermometer and the enstatite-in-clinopyroxene geothermometer may reflect in part different 'blocking temperatures' of the different geothermometers. The magnitude of NT00-C99 also exhibited a minor negative correlation with the concentration of Al_2O_3 in garnet. Large negative and positive NT00-C99 values were observed for high- and low-pressure xenolith samples, which may suggest a possible overestimation of temperature below 4 GPa and underestimation of temperature above 5 GPa. These variations may be due to biases associated

Fig. 8 Histogram showing the calculated temperature using our revised calibration of the Ni-in-garnet geothermometer (this study) (**a**), and the Nimis and Taylor (2000) enstatite-in-clinopyroxene geothermometer (**b**). Temperature estimates are made on garnet and clinopyroxene xenocryst populations from the Diavik and Ekati kimberlite pipes (see text for discussion). Ni-in-garnet temperature estimates made using our updated calibration used a fixed Ni olivine concentration of 3000 ppm. NT00 = Nimis and Taylor (2000) enstatite-in-clinopyroxene geothermometer; S21 = updated Ni-in-garnet geothermometer presented in this study. A statistically significant bin size of 50 °C was used for each histogram in Fig. 8
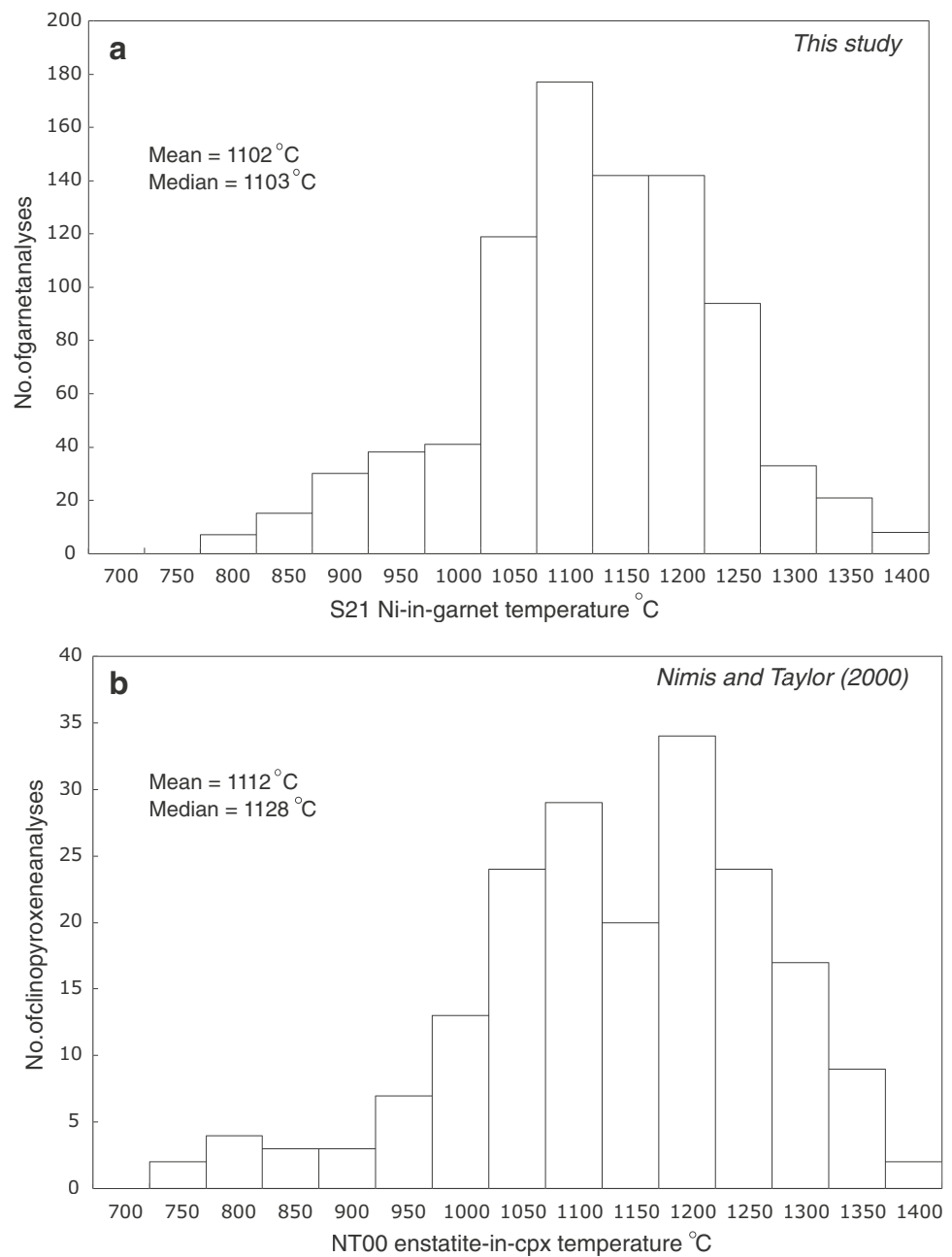
with the high-pressure, high-temperature experiments used to calibrate the Canil (1999) geothermometer.

The temperature difference between our updated calibration (Eq. 4) and the Nimis and Taylor (2000) enstatite-in-clinopyroxene geothermometer (NT00-S21) were typically ± 100 °C for most garnet grains. Temperature estimates between 1050 and 1400 °C exhibited minimal scatter, and typically correlated linearly with the Nimis and Taylor (2000) temperature estimates. Most were within ± 50 °C of the Nimis and Taylor (2000) temperature (Fig. 7c). Between

800 and 1000 °C our updated calibration typically provided temperature estimates within 150°C of the Nimis and Taylor (2000) temperature. Temperature estimates made from our updated calibration between 800 and 1000 °C were typically higher than those calculated using the Nimis and Taylor (2000) geothermometer. This trend may be a result of several factors including a slower up-take of Ni in garnet at lower temperature, or problems associated with blocking temperatures. The NT00-S21 for our updated calibration does not present any systematic correlation with the concentration of

Table 7 Summary of the descriptive statistics for the temperature estimates made on garnet and clinopyroxene xenocryst populations from the Diavik-Ekati kimberlite pipes using our revised calibration of the Ni-in-garnet geothermometer (This study) and the Nimis and Taylor (2000) enstatite-in-clinopyroxene geothermometer (NT00)

	This study	NT00
Mean	1102	1111
Standard error	4.03	9.49
Median	1103	1128
Standard deviation	114	131
Kurtosis	0.27	0.29
Skewness	− 0.32	− 0.60
Range	673	679
Minimum	758	712
Maximum	1432	1391
Count	807	191

major oxides in garnet. In addition, the variation in NT00-S21 does not exhibit any resolvable correlation with pressure, which confirms that our updated calibration can be confidently applied to compositionally diverse peridotitic garnet xenocrysts and xenoliths derived from the mantle at pressures of ~ 2 GPa to > 7 GPa.

Application to single-grain garnet xenocrysts

To further evaluate our new calibration of the Ni-in-garnet geothermometer we calculate the Ni-in-garnet equilibration temperature for a large population of single-grain garnet xenocrysts derived from mantle peridotite xenoliths from the diamondiferous Eocene (50–55 Ma) Diavik and Ekati kimberlite pipes of the Lac de Gras kimberlite field in the Northwest Territories of Canada. These pipes provide an ideal test of the Ni-in-garnet geothermometer because they have been extensively characterised over the past two decades (Bostock 1998; Griffin et al. 1999, 2004; Creighton et al. 2010; Aulbach et al. 2013; Snyder et al. 2014), such that the equilibration temperature and pressure of xenoliths and xenocryst are well-established. Mineral analyses for garnet have been taken from Griffin et al. (2004) and an unpublished dataset of Diavik garnet concentrate listed in Supplementary File 2 (Yaxley, unpubl.). The combined datasets contain over 800 garnet analyses. We have calculated the equilibration temperature for garnet using our updated calibration (Eq. 4) using a fixed olivine Ni concentration of 3000 ppm. Equilibration pressure and temperature were also calculated for a large population of single-grain clinopyroxene xenocrysts using the Nimis and Taylor (2000) enstatite-in-clinopyroxene geothermometer and the recent experimentally recalibrated chromium-in-clinopyroxene geobarometer

(Sudholz et al. 2021). Clinopyroxene xenocryst PT estimates are taken from the published datasets discussed in Sudholz et al. (2021). This dataset contains approximately 190 PT estimates (Sudholz et al. 2021 references therein).

The estimated equilibration temperature for the Diavik–Ekati garnet and clinopyroxene xenocrysts are approximately evenly distributed for each of the two geothermometer calibrations (Fig. 8a: This study; Fig. 8b: Nimis and Taylor 2000). Both calibrations exhibited a similar temperature range (maximum temperature-minimum temperature) between 673 and 679 °C. The kurtosis and skewness for the calibrations ranged between 0.27–0.29 and − 0.60 to − 0.32, respectively. A summary of the descriptive statistics for Fig. 8 are shown in Table 7. The ranges in temperature estimates for our updated calibration (758–1432 °C) and the Nimis and Taylor (2000) enstatite-in-clinopyroxene geothermometer (712–1391 °C) are very similar and thus should enable confident use of temperature estimates derived from the updated Ni-in-garnet geothermometer with those from pyroxene geothermometry.

Conclusion

Experimental methods have been used to revisit Ni partitioning between garnet and olivine in peridotite. LA-ICP-MS and EPMA data for nine new piston cylinder diffusion experiments conducted at 2.25–4.5 GPa and 1100–1325 °C have been used to recalibrate the Ni-in-garnet geothermometer. Our updated Ni-in-garnet geothermometer uses the Ni concentration (ppm) in garnet and olivine and includes X_{grt}^{Ca} and X_{grt}^{Cr} to account for the effect of CaO and Cr_2O_3 in garnet to solve for temperature. Application of our updated calibration confirms the earlier experimental calibration of the Ni-in-garnet geothermometer by Canil (1994, 1999). Comparison with the experimental datasets and several large natural peridotite xenolith datasets shows an improvement in precision and accuracy of our revised calibration of the Ni-in-garnet geothermometer relative to existing versions of the geothermometer. Our updated calibration can be used as a single grain geothermometer on garnet xenocrysts derived from disaggregated peridotitic source rocks by assuming a fixed olivine Ni concentration of 3000 ppm. We anticipate that our revised calibration will enable more confident use of the Ni-in-garnet geothermometer in studies of the nature of the upper mantle and assessment of its diamond potential.

References

Agashev A, Ionov D, Pokhilenko N, Golovin A, Cherepanova Y, Sharygin I (2013) Metasomatism in lithospheric mantle roots: constraints from whole-rock and mineral chemical composition of deformed peridotite xenoliths from kimberlite pipe Udachnaya. Lithos 160:201–215

Aulbach S, Griffin WL, Pearson NJ, O'Reilly SY (2013) Nature and timing of metasomatism in the stratified mantle lithosphere beneath the central Slave craton (Canada). Chem Geol 352:153–169

Bose K, Ganguly J (1995) Quartz-coesite transition revisited: reversed experimental determination at 500–1200 C and retrieved thermochemical properties. Am Miner 80(3–4):231–238

Bostock M (1998) Mantle stratigraphy and evolution of the Slave province. J Geophys Res Solid Earth 103(B9):21183–21200

Bussweiler Y, Brey G, Pearson D, Stachel T, Stern R, Hardman M, Kjarsgaard B, Jackson S (2017) The aluminum-in-olivine thermometer for mantle peridotites—experimental versus empirical calibration and potential applications. Lithos 272:301–314

Canil D (1994) An experimental calibration of the "Nickel in Garnet" geothermometer with applications. Contrib Miner Petrol 117(4):410–420

Canil D (1999) The Ni-in-garnet geothermometer: calibration at natural abundances. Contrib Miner Petrol 136(3):240–246

Canil D, StC OH (1996) Distribution of ferric iron in some upper-mantle assemblages. J Petrol 37(3):609–635

Carlson WD (2012) Rates and mechanism of Y, REE, and Cr diffusion in garnet. Am Miner 97:1598–1618

Creighton S, Stachel T, Eichenberg D, Luth RW (2010) Oxidation state of the lithospheric mantle beneath Diavik diamond mine, central Slave craton, NWT. Can Contrib Mineral Petrol 159(5):645–657

De Hoog JC, Gall L, Cornell DH (2010) Trace-element geochemistry of mantle olivine and application to mantle petrogenesis and geothermobarometry. Chem Geol 270(1–4):196–215

Doucet LS, Ionov DA, Golovin AV (2015) Paleoproterozoic formation age for the Siberian cratonic mantle: Hf and Nd isotope data on refractory peridotite xenoliths from the Udachnaya kimberlite. Chem Geol 391:42–55

Gibson SA, Malarkey J, Day JA (2008) Melt depletion and enrichment beneath the western Kaapvaal Craton: evidence from Finsch peridotite xenoliths. J Petrol 49(10):1817–1852

Green DH (2015) Experimental petrology of peridotites, including effects of water and carbon on melting in the Earth's upper mantle. Phys Chem Miner 42(2):95–122

Grégoire M, Bell D, Le Roex A (2003) Garnet lherzolites from the Kaapvaal Craton (South Africa): trace element evidence for a metasomatic history. J Petrol 44(4):629–657

Griffin W, Ryan C (1995) Trace elements in indicator minerals: area selection and target evaluation in diamond exploration. J Geochem Explor 53(1–3):311–337

Griffin W, Cousens D, Ryan C, Sie S, Suter G (1989) Ni in chrome pyrope garnets: a new geothermometer. Contrib Miner Petrol 103(2):199–202

Griffin W, Doyle B, Ryan C, Pearson N, Suzanne YOR, Davies R, Kivi K, Van Achterbergh E, Natapov L (1999) Layered mantle lithosphere in the Lac de Gras area, Slave craton: composition, structure and origin. J Petrol 40(5):705–727

Griffin W, O'Reilly SY, Doyle B, Pearson N, Coopersmith H, Kivi K, Malkovets V, Pokhilenko N (2004) Lithosphere mapping beneath the North American plate. Lithos 77(1–4):873–922

Grütter HS, Gurney JJ, Menzies AH, Winter F (2004) An updated classification scheme for mantle-derived garnet, for use by diamond explorers. Lithos 77(1–4):841–857

Hanger BJ, Yaxley GM, Berry AJ, Kamenetsky VS (2015) Relationships between oxygen fugacity and metasomatism in the Kaapvaal subcratonic mantle, represented by garnet peridotite xenoliths in the Wesselton kimberlite, South Africa. Lithos 212:443–452

Holloway JR, Pan V, Gudmundsson G (1992) High-pressure fluid-absent melting experiments in the presence of graphite: oxygen fugacity, ferric/ferrous ratio and dissolved CO2. Eur J Mineral 4(1):105–114

Ionov D (2004) Chemical variations in peridotite xenoliths from Vitim, Siberia: inferences for REE and Hf behaviour in the garnet-facies upper mantle. J Petrol 45(2):343–367

Ionov DA, Doucet LS, Ashchepkov IV (2010) Composition of the lithospheric mantle in the Siberian craton: new constraints from fresh peridotites in the Udachnaya-East kimberlite. J Petrol 51(11):2177–2210

Jochum KP, Weis U, Stoll B, Kuzmin D, Yang Q, Raczek I, Jacob DE, Stracke A, Birbaum K, Frick DA (2011) Determination of reference values for NIST SRM 610–617 glasses following ISO guidelines. Geostand Geoanal Res 35(4):397–429

Köhler TP, Brey GP (1990) Calcium exchange between olivine and clinopyroxene calibrated as a geothermobarometer for natural peridotites from 2 to 60 kb with applications. Geochim Cosmochim Acta 54(9):2375–2388

Le Roex A, Class C (2016) Metasomatic enrichment of Proterozoic mantle south of the Kaapvaal Craton, South Africa: origin of sinusoidal REE patterns in clinopyroxene and garnet. Contrib Miner Petrol 171(2):14

Luth RW, Virgo D, Boyd FR, Wood BJ (1990) Ferric iron in mantle derived garnets: implications for thermobarometry and for the oxidation state of the mantle. Contrib Miner Petrol 104:56–72

Matjuschkin V, Brey GP, Höfer HE, Woodland AB (2014) The influence of Fe 3+ on garnet–orthopyroxene and garnet–olivine geothermometers. Contrib Miner Petrol 167(2):972

Nimis P, Grütter H (2010) Internally consistent geothermometers for garnet peridotites and pyroxenites. Contrib Miner Petrol 159(3):411–427

Nimis P, Taylor WR (2000) Single clinopyroxene thermobarometry for garnet peridotites. Part I. Calibration and testing of a Cr-in-Cpx barometer and an enstatite-in-Cpx thermometer. Contrib Mineral Petrol 139(5):541–554

O'Neill HSC, Wood B (1979) An experimental study of Fe-Mg partitioning between garnet and olivine and its calibration as a geothermometer. Contrib Miner Petrol 70(1):59–70

Paton C, Hellstrom J, Paul B, Woodhead J, Hergt J (2011) Iolite: Freeware for the visualisation and processing of mass spectrometric data. J Anal At Spectrom 26(12):2508–2518

Pouchou J-L, Pichoir F (1991) Quantitative analysis of homogeneous or stratified microvolumes applying the model "PAP". In: Electron probe quantitation, Springer, pp 31–75

Ryan CG, Griffin WL, Pearson NJ (1996) Garnet geotherms: pressure-temperature data from Cr-pyrope garnet xenocrysts in volcanic rocks. J Geophys Res Solid Earth 101(B3):5611–5625

Snyder D, Hillier M, Kjarsgaard B, De Kemp E, Craven J (2014) Lithospheric architecture of the Slave craton, northwest Canada, as determined from an interdisciplinary 3-D model. Geochem Geophys Geosyst 15(5):1895–1910

Sudholz Z, Yaxley G, Jaques A, Brey G (2021) Experimental recalibration of the Cr-in-clinopyroxene geobarometer: improved precision and reliability above 4.5 GPa. Contrib Mineral Petrol 176(2):1–20

van Achterbergh E, Griffin WL, Stiefenhofer J (2001) Metasomatism in mantle xenoliths from the Letlhakane kimberlites: estimation of element fluxes. Contrib Miner Petrol 141(4):397–404

Viljoen K, Schulze D, Quadling A (2005) Contrasting group I and group II eclogite xenolith petrogenesis: petrological, trace element and isotopic evidence from eclogite, garnet-websterite and alkremite xenoliths in the Kaalvallei kimberlite, South Africa. J Petrol 46(10):2059–2090

Viljoen F, Dobbe R, Smit B (2009) Geochemical processes in peridotite xenoliths from the Premier diamond mine, South Africa: evidence for the depletion and refertilisation of subcratonic lithosphere. Lithos 112:1133–1142

Yaxley GM, Green DH (1998) Reactions between eclogite and peridotite: mantle refertilisation by subduction of oceanic crust. Schweiz Mineral Petrogr Mitt 78(2):243–255

Yaxley GM, Berry AJ, Kamenetsky VS, Woodland AB, Golovin AV (2012) An oxygen fugacity profile through the Siberian Craton—Fe K-edge XANES determinations of $Fe^{3+}/\sum Fe$ in garnets in peridotite xenoliths from the Udachnaya East kimberlite. Lithos 140:142–151

Zheng J, Griffin WL, O'reilly SY, Yang J, Li T, Zhang M, Zhang RY, Liou JG (2006) Mineral chemistry of peridotites from paleozoic, mesozoic and cenozoic lithosphere: constraints on mantle evolution beneath eastern China. J Petrol 47(11):2233–2256

Ziberna L, Nimis P, Zanetti A, Marzoli A, Sobolev NV (2013) Metasomatic processes in the central Siberian cratonic mantle: evidence from garnet xenocrysts from the Zagadochnaya kimberlite. J Petrol 54(11):2379–2409

Authors and Affiliations

Z. J. Sudholz[1] · G. M. Yaxley[1] · A. L. Jaques[1] · J. Chen[2]

✉ Z. J. Sudholz
  Zachary.sudholz@anu.edu.au

[1] Research School of Earth Sciences, Australian National University, Canberra, ACT 2601, Australia

[2] Centre for Advanced Microscopy, Australian National University, Canberra, ACT 2601, Australia